Recycled polycarbonate and polycarbonate/acrylonitrile butadiene styrene feedstocks for circular economy product applications with fused granular fabrication-based additive manufacturing

Alessia Romani [1, 2, 3], Marinella Levi [2], Joshua M. Pearce [1, 4,*]

1 Dep. of Electrical & Computer Engineering, Western University, London, ON, Canada
2 Dep. of Chemistry, Materials and Chemical Engineering "Giulio Natta", Politecnico di Milano, Piazza Leonardo da Vinci 32, 20133, Milano, Italy
3 Design Department, Politecnico di Milano, Via Durando, 20158, Milano, Italy
4 Ivey Business School, Western University, London, ON, Canada

alessia.romani@polimi.it; marinella.levi@polimi.it
** contact author: joshua.pearce@uwo.ca*

Abstract

Distributed recycling and additive manufacturing (DRAM) holds enormous promise for enabling a circular economy. Most DRAM studies have focused on single thermoplastic waste stream. This study takes three paths forward from the previous literature: 1) expanding DRAM into high-performance polycarbonate/ acrylonitrile butadiene styrene (PC/ABS) blends, 2) extending PC/ABS blend research into both recycled materials and into direct fused granular fabrication (FGF) 3-D printing and 3) demonstrating the potential of using recycled PC/ABS feedstocks for new applications in circular economy contexts. A commercial open source large-format FGF 3-D printer was modified and used to assess the different printability and accuracy of recycled PC and PC/ABS. The mechanical properties (tensile and impact) following the ASTM D638 and D6110-18 standards were quantified. A weather simulation test (ASTM D5071-06) was performed to assess outdoor performance. Finally, two applications in sporting goods and furniture were demonstrated. In general, better printability was achieved with recycled PC/ABS compared to recycled PC, as well as good dimensional accuracy at printing speeds of 30 and 40 mm/s. Minimal qualitative differences and discoloration were visible on the samples after accelerated weather exposure, with results in accordance with the state-of-the-art. The rPC/ABS results from tensile tests show similar values to those of rPC for elastic modulus (2.1 ± 0.1 GPa), tensile strength (41.6 ± 6.3 MPA), and elongation at break (2.8 ± 0.9 %), which are also comparable with previous studied virgin 3-D printed filaments. Similarly, impact energy (115.78 ± 24.40 kJ/m^2) and resistance values (810.36 ± 165.77 J/m) are comparable in the two tested formulations, reaching similar results compared to FFF 3-D printed filaments, as well as virgin materials for injection molding. Finally, the two demonstration products in the sporting goods and furniture sectors were successfully fabricated with rPC/ABS, achieving complex patterns and good printing speeds for recycled feedstocks. It is concluded rPC/ABS blends represent a potential high-performance feedstock for DRAM, validating its use in direct FGF 3-D printing systems and potential applications for a circular economy.

Keywords: 3-D printing; Recycling; Fused Filament Fabrication (FFF); Fused Granular Fabrication (FGF); Distributed Recycling for Additive Manufacturing (DRAM); Mechanical properties.

Recycled polycarbonate and polycarbonate/acrylonitrile butadiene styrene feedstocks for circular economy product applications with fused granular fabrication-based additive manufacturing

Abstract

Distributed recycling and additive manufacturing (DRAM) holds enormous promise for enabling a circular economy. Most DRAM studies have focused on single thermoplastic waste stream. This study takes three paths forward from the previous literature: 1) expanding DRAM into high-performance polycarbonate/ acrylonitrile butadiene styrene (PC/ABS) blends, 2) extending PC/ABS blend research into both recycled materials and into direct fused granular fabrication (FGF) 3-D printing and 3) demonstrating the potential of using recycled PC/ABS feedstocks for new applications in circular economy contexts. A commercial open source large-format FGF 3-D printer was modified and used to assess the different printability and accuracy of recycled PC and PC/ABS. The mechanical properties (tensile and impact) following the ASTM D638 and D6110-18 standards were quantified. A weather simulation test (ASTM D5071-06) was performed to assess outdoor performance. Finally, two applications in sporting goods and furniture were demonstrated. In general, better printability was achieved with recycled PC/ABS compared to recycled PC, as well as good dimensional accuracy at printing speeds of 30 and 40 mm/s. Minimal qualitative differences and discoloration were visible on the samples after accelerated weather exposure, with results in accordance with the state-of-the-art. The rPC/ABS results from tensile tests show similar values to those of rPC for elastic modulus (2.1 ± 0.1 GPa), tensile strength (41.6 ± 6.3 MPA), and elongation at break (2.8 ± 0.9 %), which are also comparable with previous studied virgin 3-D printed filaments. Similarly, impact energy (115.78 ± 24.40 kJ/m^2) and resistance values (810.36 ± 165.77 J/m) are comparable in the two tested formulations, reaching similar results compared to FFF 3-D printed filaments, as well as virgin materials for injection molding. Finally, the two demonstration products in the sporting goods and furniture sectors were successfully fabricated with rPC/ABS, achieving complex patterns and good printing speeds for recycled feedstocks. It is concluded rPC/ABS blends represent a potential high-performance feedstock for DRAM, validating its use in direct FGF 3-D printing systems and potential applications for a circular economy.

Keywords: 3-D printing; Recycling; Fused Filament Fabrication (FFF); Fused Granular Fabrication (FGF); Distributed Recycling for Additive Manufacturing (DRAM); Mechanical properties.

1. Introduction

The global plastic waste problem [1] has the potential to be aggravated by the rapid rise of 3-D printing waste products [2]. Although the first self-replicating rapid prototyper (RepRap) [3-5] released as an open source 3-D printer resulted in rapid innovation, cost reductions, and the democratization of additive manufacturing (AM) [6-8], a concerning amount of 3-D printing plastic waste is landfilled [9] as the global 3-D printing market is going to reach $7.7 billion by 2024 [10]. A superior approach to a linear material process, even if distributed, is to target a circular economy for AM [11,12]. This can be done by using the distributed recycling for additive manufacturing (DRAM) model [13-15]. In the DRAM model prosumers (producing consumers) save or make money when recycling with DRAM, as opposed to complete lack of personal financial incentive in traditional recycling models [13]. Prosumers following DRAM can use both AM waste and traditional plastic waste to produce 3-D printing feedstocks, which are generally worth $20/kg as opposed to $1-5/kg for plastic scrap. By producing either the feedstock or even more valuable 3-D printed products, directly where they are consumed, there are substantive environmental benefits [16-18]. DRAM prosumers can generally save substantial money per product [19,20] and obtain an extremely high return on investment [21]. The DRAM approach can be applied globally [22] and thus could have a major impact on global value chains [23].

DRAM research started and for some time has centered on the use of some type of recyclebot, which is a waste plastic extruder [24,25] that manufacturers filament to be used in fused filament fabrication (FFF)-based low-cost 3-D printers. Recyclebot-based DRAM has been demonstrated for a wide range of single polymer materials: acrylonitrile butadiene styrene (ABS) [22,26-29], polylactic acid (PLA) [25,30], high-density polyethylene (HDPE) [31,32], and polyethylene terephthalate (PET) [33]. Only a few studies, however, looked at the potential of making filament from composites or blends [35-38]. When using the recyclebot-to-3-D printing filament method for each cycle of materials, there are two melt and solidification sub-cycles. Each sub-cycle reduces the length of the polymer chains, which weakens the material until by approximately the fifth full cycle the material properties have degraded enough that an intervention is necessary [34]. Another approach, with more promise to extend the lifetime of recyclable polymers in the DRAM context is to use direct extrusion-based waste 3-D printing. This can be done via fused granular fabrication (FGF)/fused particle fabrication (FPF) for a number of plastics including polypropylene (PP) [39], PET [40]; PLA [41,42], and ABS [43]. There are a number of commercial large-format 3-D printers (GigabotXLT, Exabot, Terabot, The BoX, T3500, 400 series, BIG-meter, BigRep One, F1000) [44-52], waste hangprinters

[53,54] that can be used in DRAM and the use of these printers for DRAM is gaining attention for the potential to foster new applications, i.e., furniture and building. A limited range of recycled feedstocks, however, is currently considered within this context.

FPF/FGF has also been demonstrated with the higher strength single polymers such as polycarbonate (PC), which also allows for molding of lower melting temperatures and the use of materials that are less easily processed by AM [55]. PC, however, has disadvantages, such as poor processability, hygroscopic behavior, low scratch resistance, and high production costs [56]. These disadvantages can be overcome using a blend of PC and ABS, improving the processability of PC and keeping good tensile, impact, and flexural properties [57,58]. PC/ABS blends usually show good heat resistance and high values of impact strength and toughness [59]. Focusing on FFF systems, parts made of PC/ABS filaments reach good mechanical properties, such as elastic moduli and tensile strength [60,61], despite the strong influence of interlayer adhesion and building orientation of 3-D printed samples [62]. Although the increasing interest in recycling engineering polymers for new applications in 3-D printing, no previous works were found on the use of PC/ABS feedstock on FGF systems, as well as recycled blends on FFF/FGF 3-D printers. The processability of PC/ABS after multiple reprocessing cycles was previously assessed only for injection molding [63], showing a knowledge gap for FFF/FGF systems.

This study thus takes three paths forward from the previous literature. First it expands the DRAM work into high performance PC/ABS blends. Second, it extends the PC/ABS blend research into both recycled materials and into direct FGF 3-D printing. Thus, this work investigates the use of recycled PC and PC/ABS blend with large-format open source FGF 3-D printing system. Finally, the aim is to demonstrate the potential of using recycled PC/ABS feedstocks for new applications in circular economy contexts, exploiting its use with large-format 3-D printers. A commercial open source large-format FGF 3-D printer was modified and used to assess the different printability and accuracy of recycled PC and recycled PC/ABS as a preliminary step. The mechanical properties (tensile and impact) following the ASTM D638 and D6110-18 standards were quantified. A weather simulation test (ASTM D5071-06) was then performed to assess the influence of weather to allow for outdoor potential applications. Finally, two application fields were selected for the development of two new products to demonstrate the feasibility of using recycled feedstock for real applications, i.e., protective sports equipment and customizable furniture. To this end, recycled PC and PC/ABS feedstock can potentially foster the design of new products by widening the range of possible application fields to more technical sectors and accessible products.

2. Methods

2.1 *Materials*

Recycled polycarbonate (rPC) feedstock was provided by Advanced Composites (Sidney, OH, US) in the form of shredded shards and particles. This recycled feedstock was sorted with a 3 mm mesh size sieve to obtain a relatively uniform granulometry of the material. Recycled acrylonitrile butadiene styrene (rABS) from McDunnough (Fenton, MI, US) was used in the form of pellets as provided. Two different materials were tested within this work: 100% wt. of rPC feedstock and a blend of rPC and rABS. In detail, the rPC/ABS blend was composed of 70% wt. of rPC feedstock and 30% wt. of rABS pellets. This percentage was selected by considering the state of the art in 3-D printed PC/ABS blends with FFF and FGF systems [57,64,65], as well as the aim to maximize the percentage of rPC feedstock of the blend and increase its mechanical properties.

2.2 *Printability comparison tests*

The accuracy of the FGF 3-D printing system was assessed through a comparison of different variations of a 3-D printed sample, designed to evaluate the printability and accuracy of the system with recycled feedstock (Fig. 1). This sample has a nominal dimension of 87x45x45 mm. Its shape comprises some perpendicular walls for wall thickness measurements and some overhang walls to verify the shape retention after the extrusion of each layer. The sample designs were sliced with the open source PrusaSlicer (Prusa Research, Prague, Czech Republic) [66], and all designs for this study are available on the Open Science Framework (OSF) under GNU General Public License (GPL) 3.0 [67]. The sample was sliced by combining different printing speeds (20, 30, and 40 mm/s) with a layer height of 0.4 mm, which means ½ of the nozzle diameter, obtaining a batch of three combinations for each material, six different sets of 3-D printed pieces in total. The other printing parameters were kept constant for each gcode and are summarized in Table 1 (rPC) and Table 2 (rPC/ABS). The 3-D printed samples were visually inspected and measured to obtain experimental values to compare with the nominal ones. The comparisons were performed on the weight, overall dimensions, and wall thickness. The nominal weight values were estimated by calculating the density of rPC (1.2 g/cm^3) and rPC/ABS (1.15 g/cm^3) and inserting the values in PrusaSlicer. The values were then used to assess the absolute error of the 3-D printer at different layer heights and printing speeds, resulting in two comparative matrixes.

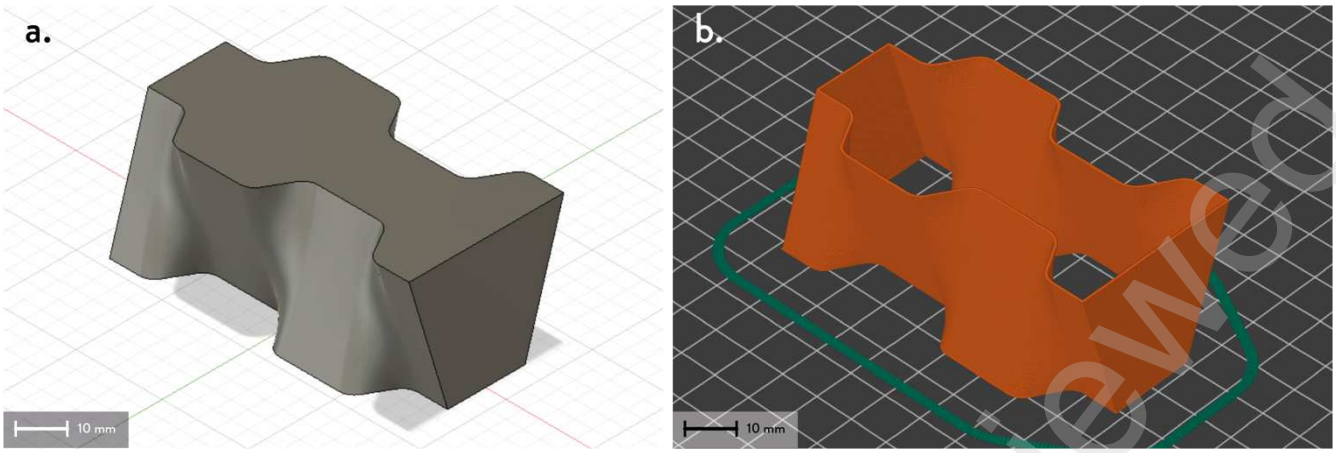

Fig. 1. Printability test design: (a) CAD preview of the STEP file and (b) gcode preview.

Table 1. Main 3-D printing parameters - recycled PC.

Parameters	Unit	Brick samples	Tensile tests	Impact tests	UV tests
Nozzle diameter	mm	0.8	0.8	0.8	0.8
Layer height	mm	0.2 – 0.4	0.3	0.3	0.3
Speed	mm/min	20, 30, 40	25	30	40
Wall line count – perimeters	//	1	2	2	2
Extrusion temperature	°C	250 (H1), 235 (H2), 220 (H3)	250 (H1), 235 (H2), 220 (H3)	250 (H1), 235 (H2), 220 (H3)	250 (H1), 235 (H2), 220 (H3)
Bed temperature	°C	110	110	110	110
Flow	%	90	80	70	60
Cooling fan	%	0	0	0	0

Table 2. Main 3-D printing parameters - recycled PC/ABS.

Parameters	Unit	Brick samples	Tensile tests	Impact tests	UV tests	Application (Sports)	Application (Furniture)
Nozzle diameter	mm	0.8	0.8	0.8	0.8	0.8	0.8
Layer height	mm	0.2 – 0.4	0.3	0.3	0.3	0.4	0.4
Speed	mm/min	20, 30, 40	30	20	30	30	40
Wall line count – perimeters	//	1	2	2	2	3	2
Infill percentage	%	0	100	100	100	0	10
Extrusion temperature	°C	240 (H1), 230 (H2), 215 (H3)	240 (H1), 230 (H2), 215 (H3)	240 (H1), 230 (H2), 215 (H3)	240 (H1), 230 (H2), 215 (H3)	240 (H1), 230 (H2), 215 (H3)	240 (H1), 230 (H2), 215 (H3)
Bed temperature	°C	110	110	110	110	110	110
Flow	%	80	60	40	50	60	60
Cooling fan	%	0	0	0	0	0	0

2.3 Weather simulation test

The possible photodegradation effects of weather on 3-D printed rPC and rPC/ABS were preliminarily evaluated through simulated weathering experiments, helping in narrowing down the possible range of applications of the tested materials. The simulation was done using the Xenon Arc apparatus Q-Sun Xenon Test Chamber Model Xe-3 (Q-Lab Corporation, Westlake,

OH, USA) equipped with a sunlight simulation lamp and following the ASTM Standard D5071-06 [68]. Two different batches of five squared samples each (nominal dimensions: 70x70x3 mm) were 3-D printed using the printing parameters shown in Table 1 (rPC) and Table 2 (rPC/ABS). An additional sample of commercial injection-molded PC/ABS was used as a control material during the simulation. The surface of each sample was cleaned with methanol before positioning them into the testing chamber with some tape. The simulation was performed by following the parameters of Cycle 2 for 24h, simulating exposures with slight moisture stresses. The main cycle (2h in total) consists of a continuous light time of 102 min and 18 min of light and water spray conducted with a temperature of 63°C, relative humidity of 60%, and irradiance of 0.35 W/(m^2·nm) at 340 nm.

To detect some physical changes due to the simulation, a colorimetry test was conducted on the specimens before and after their exposure in the Xenon Arc apparatus by means of a spectrophotometer (Spectro2guide from BYK Additives & Instruments, Wesel, Germany), following the ASTM Standard D2244-21 [69]. Each sample was cleaned with methanol before measuring the L*a*b* coordinates of the CIELAB color space, where L* means lightness, and a* and b* the color coordinates. Five different points for each sample were measured, obtaining the mean values and standard deviations of the L*a*b* coordinates before and after the weather simulation test. The direction of the color difference ΔL*, Δa*, Δb* and the discoloration ΔE* were then calculated by using equations 1-4,

$$\Delta L^* = L^*_B - L^*_S \quad \text{Eq. 1}$$

$$\Delta a^* = a^*_B - a^*_S \quad \text{Eq. 2}$$

$$\Delta b^* = b^*_B - b^*_S \quad \text{Eq. 3}$$

$$\Delta E^* = \sqrt{(\Delta L^*)^2 + (\Delta a^*)^2 + (\Delta b^*)^2} \quad \text{Eq. 4}$$

where L^*_B, a^*_B, and b^*_B are the coordinates after the test, and L^*_S, a^*_S, and b^*_S before the test. The signs of ΔL*, Δa*, Δb* give an overall idea of the difference in colors according to the following path: +ΔL* lighter, -ΔL* darker, +Δa* redder, -Δa* greener, +Δb* yellower, -Δb* bluer. The spectrophotometer was also used to measure the gloss of the sample surfaces before and after the weather simulation test with a 60° geometry, expressing the results in Gloss Units (GU). Five different measurements were performed on each sample, allowing to calculate the mean values and standard deviations.

2.4 Tensile tests

Tensile tests were carried out using a Zwick Roell Z010 testing machine (ZwickRoell GmbH & Co. KG, Ulm, Germany) equipped with a 10 kN cell load and an extensometer, following the ASTM standard D638-22 [70]. Tests were performed at a speed of 1 mm/min. Two batches of ten Type IV samples (33 mm of gauge length, 4 mm of thickness, and 6 mm of width) were fabricated following the parameters shown in Table 1 (rPC) and Table 2 (rPC/ABS) [71,72]. To avoid interlayer voids, the specimens were printed with a 100% rectilinear infill. In case of asperities on the top layers, they were manually removed by sanding to reach a constant cross-section in the gauge length. The actual thickness and width were then measured with a caliper. After testing, the mean values and standard errors of stress, strain, and elastic modulus were calculated from the stress-strain curves obtained in the tests.

2.5 Impact tests

Impact tests were performed with a Charpy impact tester (Instron, Norwood, MA, USA) following the ASTM standard D6110-18 [73] with a span of 40 mm. A pendulum of 30 kg with a capacity of 252 J was used for the tests (length of 1.3 m and angle of 70°). Two batches of ten notched samples were 3-D printed using the parameters of Table 1 (rPC) and Table 2 (rPC/ABS). Their overall dimensions are 12.7x63.5x6.5 mm. The notch has a maximum nominal depth of 2.6 mm and an angle of 45°. As for tensile bars, the samples were printed with a 100% rectilinear infill, and the main asperities were manually sanded when interfering with the notch geometry. The actual widths and depths under the notch were measured with a caliper for each specimen. The machine was calibrated before conducting the tests by raising and releasing the pendulum without loading any sample. The mean net breaking energy and impact energy values, as well as their standard deviations, were calculated starting from the experimental results of the test.

2.6 Fracture analysis

The morphology of the fracture cross-section surface was evaluated by using microscope micrographs performed with a Keyence VHX-6000 Digital Microscope (Keyence, Mississauga, ON, Canada). Two batches of fracture cross-sections were considered for the analysis, which means the surfaces from impact specimens of rPC and rPC/ABS. At least two fracture surfaces for each sample batch were observed. The samples were observed at 100 x magnification.

2.7 Application case studies

Some applications were chosen after the printability and material characterization tests were completed. The aim was to demonstrate the use of rPC and rPC/ABS, as well as the FGF 3-D printer system, for real applications, reducing the gap between experimental studies and practical implementations. Two different case studies were selected, which correspond to different application fields: protective sports equipment and customizable furniture, resulting in two products with functional purposes. The 3-D models of the protective equipment product were designed with Grasshopper plugin for Rhinoceros 7 (Robert McNeel & Associates, Seattle, WA, USA), which helped in optimizing the shape of the models by considering the possible extrusion path of the 3-D printing hot end. The 3-D model of the customizable furniture (coat hanger joint) was previously designed and used to test large-scale cable-robot-based hangprinting systems by Rattan et al. [54]. More details about the selection criteria of the two fields, the design constraints, and the rationale behind the development process are in the Results and Discussion section. The gcode files to fabricate the two products were done using PrusaSlicer, [66], and the main parameters for both applications are visible in Table 1 (rPC) and Table 2 (rPC/ABS). The open-source designs in native CAD format, STEP and STL are available in the OSF repository [67].

2.8 3-D Printing setup redesign and parameters

The 3-D printing system used in this work is a Gigabot XLT from re:3D Inc (Houston, TX, USA). This machine is a gantry FGF open-source 3-D printer controlled with Marlin Firmware [74], equipped with a pellet extruder heated by three different heating zones, hereinafter called H1, H2, and H3, and a stainless-steel conical nozzle with a diameter of 0.8 mm [40]. The building volume of Gigabot XLT is 590x760x900 mm. This means that it can be considered a large-format 3-D printer since its maximum printing volume reaches almost 1 m^3 [75]. To improve the feeding of recycled feedstock and the overall performance of the system, a new version of the extruder was developed by modifying the previous design [40]. In detail, the latest version (Fig. 2a) aims to fix four main issues:

- Facilitating the feeding of recycled feedstock by redesigning the inner shape of the 3-D printed feeder, avoiding sharp angles, and removing the crammer (Fig. 2b).
- Fixing the thermocouples on H1, H2, and H3 by using accessible spare parts such as metric inserts, screws, and ring terminals, improving the reliability of the temperatures measured from the three heating zones (Fig. 2b).
- Redesigning the 3-D printed motor spacer to improve the torque resistance of the part during the extrusion (Fig. 2d).
- Improving the insulation and protection of the heating zones from feedstock with a new 3-D printed barrel cover (Fig. 2d).

The parts were designed with Fusion 360, sliced with PrusaSlicer [66], and fabricated with an open-source Prusa i3 MK3S FFF-based 3-D printer with a 0.4 mm nozzle (Prusa Research, Prague, Czech Republic). PETG and ASA were selected to manufacture the parts with a 100% infill and a layer height of 0.2 mm. The BOM and stl files of the new extruder version are available in the OSF repository [67].

The main 3-D printing parameters for the Gigabot X and recycled feedstock used in this work are listed in Table 1 (rPC) and Table 2 (rPC/ABS). In addition, to improve the adhesion of rPC and rPC/ABS, some adhesive was applied with a glue stick on the heated bed. The Prusa slicer profiles with the main parameters can be found in the OSF repository [67].

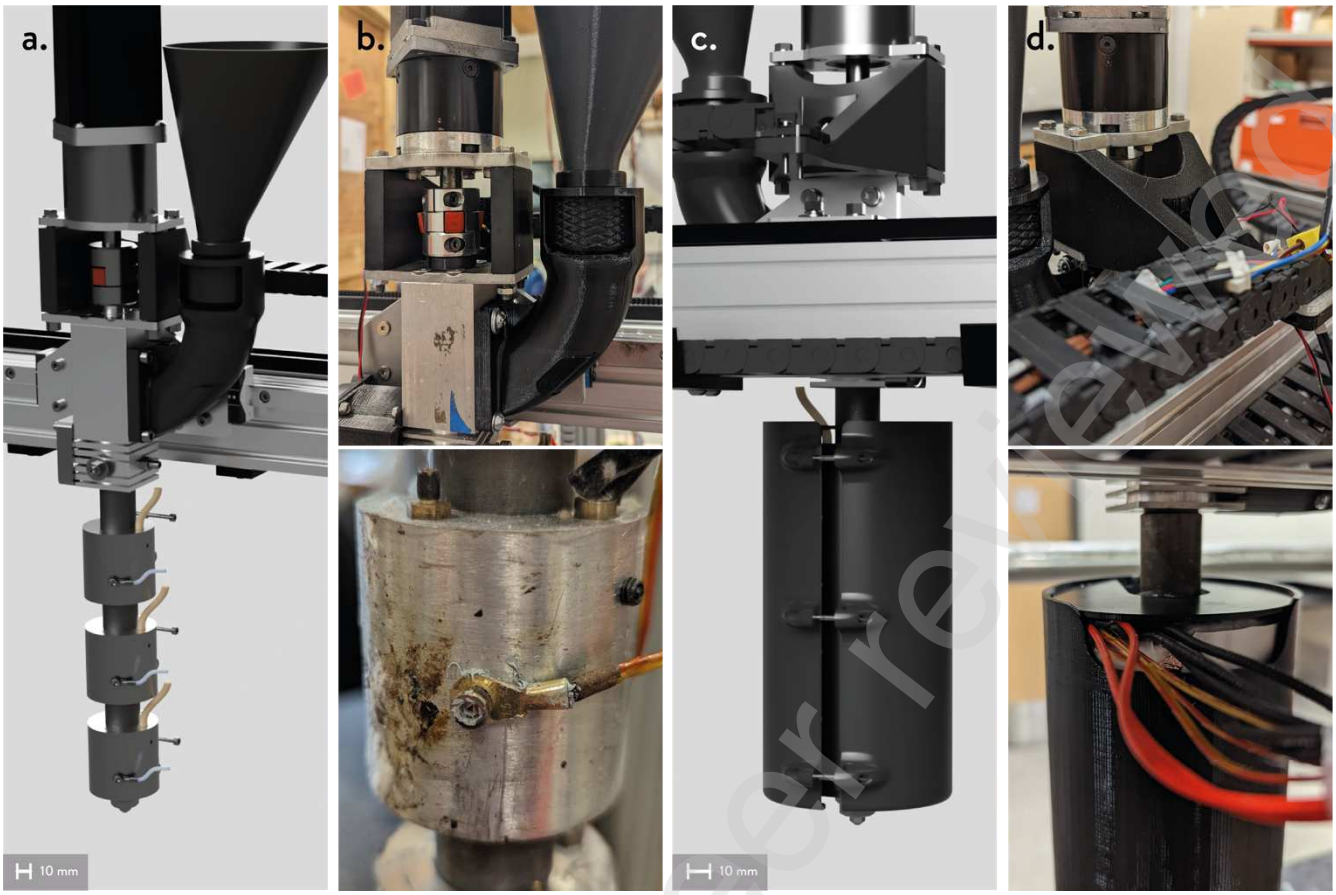

Fig. 2. New version of the GigabotX extruder: (a) preview of the assembly without insulation; (b) insight on the feeding system and thermocouple fixing; (c) preview of the assembly with insulation; and (d) insight on the motor support and insulation cover.

3. Results and Discussion

3.1 Printability comparison tests

Six different sets of 3-D printed samples (Fig. 3) were fabricated to evaluate and compare the dimensional accuracy of the extruder using recycled PC (top) and recycled PC/ABS feedstocks (bottom). After a qualitative visual inspection, some general consideration may be done. In general, the overall extrusion consistency is quite accurate, especially considering using a 100% recycled PC and a PC/ABS blend with 70% recycled PC. In other words, the variation in the feedstock granulometry linked to mechanical recycling processes is not affecting the quality of the extruded material, resulting in consistent extrusion flows for rPC and rPC/ABS. It should be noted, however, over-extrusion occurred in both cases. Focusing on recycled PC, the samples show a change in the overall quality of the extrusion according to the printing speed. Although the 3-D printed parts were successfully fabricated for each speed value, different extrusion line widths were obtained for each batch, resulting in thicker paths at lower temperatures. Furthermore, deformation occurred at lower speeds, i.e., 20 mm/s, and at higher speeds, such as 40 mm/s. The first deformation type is clearly visible from the lower accuracy in the z-axis direction and the low layer height consistency, whereas the second is linked to the slightly inclined perpendicular walls of the samples. These results may be linked to the shear rate of PC at different printing speeds, as well as the decrease in its die swelling at higher speeds after the extrusion, thus in thinner line widths [76,77]. Moreover, longer cooling times are required when using bigger nozzle diameters, affecting the overall deformation of the samples fabricated at higher printing speeds [78,79]. At the same time, the consistency of the extruded material decreased by increasing the printing speed, i.e., 40 mm/s, resulting in thinner walls and delamination between layers close to the sharp angles. This last issue may be linked to the lower interlayer adhesion at higher speeds, which means smaller bonding areas due to the thinner walls [80].

The recycled PC/ABS samples show less visible changes in the overall dimensions according to the printing speed, as well as in the extrusion line width. No signs of delamination are visible between the layers for each batch of samples, although thicker extrusion lines can be observed in the samples printed at 20 mm/s. The main reason may be the use of rABS pellet in the blend, which reduced the variability in feedstock granulometry in terms of shape, thus improving the consistency of the

extrusion flow. Furthermore, the use of rABS in this PC-rich PC/ABS blend may help in improving its printability by reducing the viscosity of PC [81].

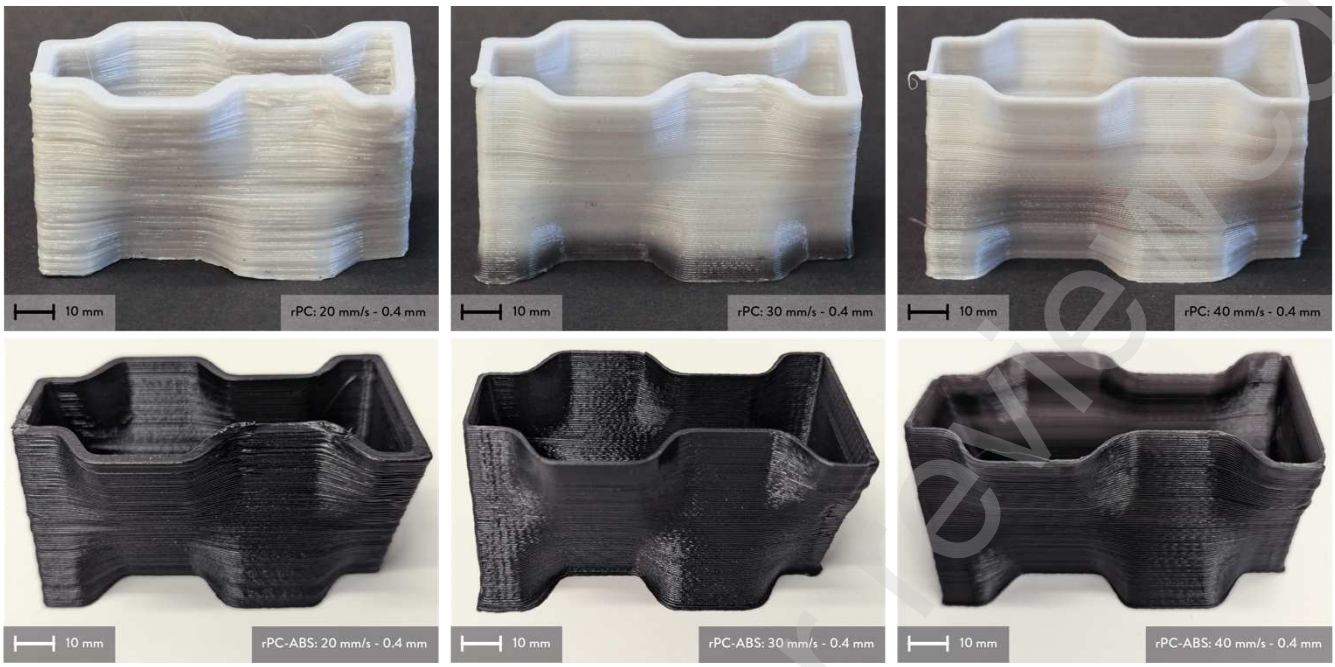

Fig. 3. 3-D printed brick samples on large-format FGF 3-D printer (layer height: 0.2 and 0.4 mm; printing speed: 20, 30, and 40 mm/s;): recycled PC (top) and recycled PC/ABS (bottom)

The overall dimensions and weight of the different batches were then measured to compare with the nominal values given by PrusaSlicer. The results of the measurements are resumed in Fig. 4, confirming the visual inspection and qualitative analysis. Less accurate measurements were obtained for samples printed at lower speeds using both materials, i.e., 20 mm/s, whereas more precise values can be seen at higher speeds.

rPC, however, exhibited higher absolute errors compared to rPC/ABS, especially considering weight and line width. The values of weight and line width at 20 mm/s of rPC were more than 200% higher than the nominal values, indicating critical over-extrusion problems. These high values in absolute error decreased by increasing the printing speed, although some over-extrusion remains at 40 mm/s. A similar trend can be seen by measuring the overall dimensions of the rPC samples despite the lower absolute and percent errors, i.e., less than 6%. Hence, the samples printed at 20 mm/s have bigger dimensions, especially length, whereas more accurate measurements were reached at 40 mm/s.

Considering rPC/ABS, more accurate values were obtained from the samples, especially at 30 and 40 mm/s, reaching lower absolute and percent errors, i.e., less than 1%. These values confirm the considerations made from the qualitative assessment, showing better printability and more consistent extrusion flow when dealing with rPC/ABS. The results also confirmed the influence of ABS pellets on the extrusion consistency. Considering the qualitative assessment and the dimensional analysis, the best compromise is reached at 30 mm/s, which provides a more consistent extrusion flow and homogeneity in the overall sample [78,79]. The recommended settings for PrusaSlicer can be found in the OSF repository [67].

	20 mm/s - 0.4 mm					30 mm/s - 0.4 mm					40 mm/s - 0.4 mm				
rPC	weight (g)	line width (mm)	length (mm)	width (mm)	height (mm)	weight (g)	line width (mm)	length (mm)	width (mm)	height (mm)	weight (g)	line width (mm)	length (mm)	width (mm)	height (mm)
Nominal values	14.35	1.2	85	45	45	14.35	1.2	85	45	45	14.35	1.2	85	45	45
Mean values	44.08	3.80	89.71	46.42	46.02	37.60	3.17	88.64	45.62	46.35	23.33	1.81	87.28	44.95	46.64
Standard Deviation	0.10	0.08	0.54	1.38	0.17	0.18	0.10	0.06	0.40	0.23	0.13	0.03	0.22	0.38	0.93
Absolute error	29.73	2.60	4.71	1.42	1.02	23.25	1.97	3.64	0.62	1.35	8.98	0.61	2.27	0.05	1.64
% error	207.2	216.7	5.5	3.1	2.3	162.2	164.2	4.3	1.4	3	62.5	51.1	2.7	-0.1	3.6
rPC-ABS	weight (g)	line width (mm)	length (mm)	width (mm)	height (mm)	weight (g)	line width (mm)	length (mm)	width (mm)	height (mm)	weight (g)	line width (mm)	length (mm)	width (mm)	height (mm)
Nominal values	13.75	1.2	85	45	45	13.75	1.2	85	45	45	13.75	1.2	85	45	45
Mean values	33.85	2.71	88.26	45.32	46.41	20.98	1.73	87.14	45.84	46.59	16.80	1.65	86.56	43.92	45.19
Standard Deviation	0.24	0.08	0.29	0.28	0.45	0.10	0.12	0.10	1.72	0.56	0.08	0.40	0.18	0.12	0.70
Absolute error	20.10	1.51	3.26	0.32	1.41	7.23	0.53	2.14	0.84	1.59	3.05	0.45	1.56	1.08	0.19
% error	146.2	126	3.8	0.7	3.1	52.5	43.8	2.5	1.9	3.5	22.2	37.1	1.8	-2.4	0.4

Fig. 4. Absolute error variation (weight, overall dimensions, line width) of recycled PC (top) and recycled PC/ABS (bottom). Red indicates high errors, orange indicates moderate errors, yellow indicates low errors and green indicates very low errors.

3.2 Weather simulation test

The photodegradation effects on rPC and rPC/ABS samples from their exposition to weather conditions were assessed with weather simulation tests performed according to ASTM D5071-06. Thanks to the constant temperature of the chamber, the wavelengths close to UVA, and the settings described in Section 2.3, the test can be considered as performed in accelerated sunlight weather conditions of a factor between 10 and 30 times, as shown by previous works [82,83]. Therefore, the 24h test of this work corresponds to a range between 10 and 30 days of exposure to natural sunlight weather conditions.

The samples before and after the weather simulation tests are visible in Fig. 5. Since no significant visible changes were qualitatively assessed, a colorimetry test was done to assess the change in color due to photodegradation from a quantitative point of view. The results resumed in Table 3 show minimal differences before and after the weather simulation tests. Slight discoloration (ΔE^*) happened to both samples, with a greater difference observed from the rPC samples. Even if the values of Δb^* have a negative sign, no significant trends were detected in the direction of the color difference. Only a slight decrease of lightness was noticed by analyzing the results, expressed by the negative sign of ΔL^* for both batches. This aspect may be linked to some minor photooxidation phenomena that occurred on the surface of the samples. Considering gloss measurements, similar values of GU can be seen from Table 5 before and after weather tests, showing no significant differences linked to exposure.

From the literature, yellowing phenomena, especially for ABS, were noticed after accelerated weathering tests [84,85], as well as a decrease in gloss [86], even after weeks of continuous exposures. According to the small differences detected from colorimetry, no further characterization tests were conducted on the batches after weather simulation tests. No remarkable changes in the mechanical properties of PC and PC/ABS were noticed after longer weather exposures in previous studies [86,87]. As investigated by Santos et al., significant modifications in the mechanical behavior of ABS were found only after more than 1200h of exposure in Xenon Arc apparatuses, which means more than one year of continuous exposure to sunlight [83]. Even if ABS generally shows photooxidative effects from sunlight exposure [84,85], the content of ABS represents the minor part of the blend analyzed in this work (30% wt.), hence the impact of its photodegradation on the mechanical properties is limited [86].

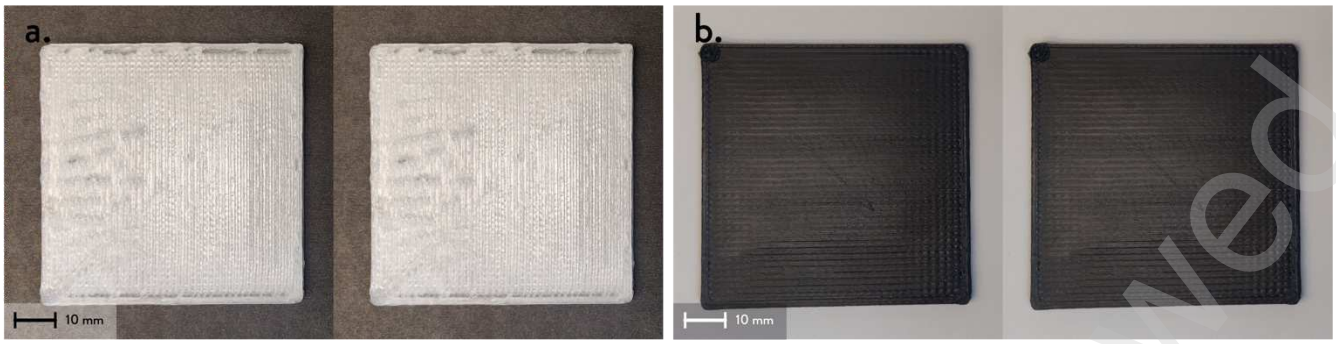

Fig. 5. Weather simulation specimens of (a) recycled PC and (b) recycled PC/ABS before (left) and after (right) conducting the test.

Table 3. Mean CIELAB L*a*b* values, ΔL*, Δ*a, Δ*b (direction of the color difference), ΔE* (discoloration), and gloss values at 60° of rPC and rPC/ABS before and after weather simulation test.

Batch		L*	a*	b*	ΔL*	Δa*	Δb*	ΔE	GU (60°)
PC/ABS (Control material)	Ref.	8.95 ± 0.13	-0.37 ± 0.05	-2.45 ± 0.28	//	//	//	//	//
rPC	Before	59.67 ± 1.86	-0.75 ± 0.02	1.33 ± 0.16	-0.50	0.07	-0.81	1.62	8.91 ± 2.14
	After	59.26 ± 1.16	-0.68 ± 0.01	0.53 ± 0.12					9.24 ± 0.65
rPC/ABS	Before	19.64 ± 0.43	-0.23 ± 0.07	-1.77 ± 0.04	-0.69	-0.01	-0.16	0.71	9.36 ± 1.05
	After	18.95 ± 0.43	-0.24 ± 0.01	-1.92 ± 0.02					9.86 ± 1.03

3.3 Tensile tests

According to the experimental tests, rPC and rPC/ABS specimens (Fig. 6a and b) exhibited brittle failure and similar mechanical behaviors. As visible in Table 4, rPC and rPC/ABS have the same elastic modulus values. In addition, tensile strength and elongation at break have comparable values, although rPC/ABS demonstrated a lower variability in results with respect to rPC (Fig. 7b and c). This result may be linked to the use of 30% wt. of rABS pellets for rPC/ABS, increasing the granulometry homogeneity of the feedstock. Hence, specimens with higher 3-D printing quality and better replicability can be printed, reducing the presence of possible interlayer voids where premature failures can occur. The mean stress-strain curves of rPC and rPC/ABS confirm the comparability of the results from the tests, especially in the first part of the curve. In this case, the low percentage of ABS in the blend, hence its rubber component, has a low influence on the decrease in the elastic modulus value [58] with similar decreasing trends of tensile strength and elongation at break [57].

Similar values of tensile strength and elongation at break were obtained for 3-D printed virgin PC/ABS blends on small-format FFF systems were observed in the literature. For example, Zhou et al. obtained tensile strength values of ~40 MPa [64]. Kannan and Ramamoorthy, and Yap et al. reached slightly higher ranges, i.e., ~43 MPa [60] and ~45 MPa [61]. This trend is also confirmed by considering the values of elongation at break, with values ranging from ~1.5% to ~4% [61,62]. Focusing on the elastic modulus, similar values were reached by Yap et al., 2.2 GPa [61], whereas lower values were shown by Kannan and Ramamoorthy and Rivet et al., i.e., ~1.7 GPa [60,62].

In general, the values with the greatest divergence were reached using a different ratio between PC and ABS, decreasing the percentage of PC, or for the high presence of interlayer porosity from the extrusion process. As a result, the over-extrusion trends from the FGF large-scale 3-D printing system may help in decreasing the interlayer porosity, hence improving the adhesion between different layers [88,78]. These values are also comparable with recycled PC/ABS blends processed with conventional manufacturing processes, i.e., injection molding, especially considering elastic modulus values [89,63]. In short, this comparison confirms the good interlayer adhesion of the samples, hence the viability of using recycled feedstock for new applications relying on manufacturing with FGF systems.

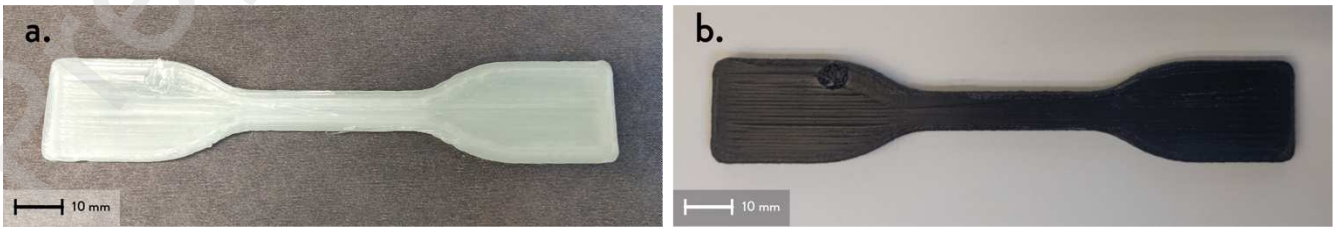

Fig. 6. Tensile specimens of (a) recycled PC and (b) recycled PC/ABS.

Table 4. Main mechanical tensile properties of 3-D printed recycled PC and recycled PC/ABS.

Batch	Elastic Modulus (GPa)	Tensile strength (MPa)	Elongation at Break (%)
Recycled PC	2.1 ± 0.1	47.0 ± 14.6	4.2 ± 1.9
Recycled PC/ABS	2.1 ± 0.1	41.6 ± 6.3	2.8 ± 0.9

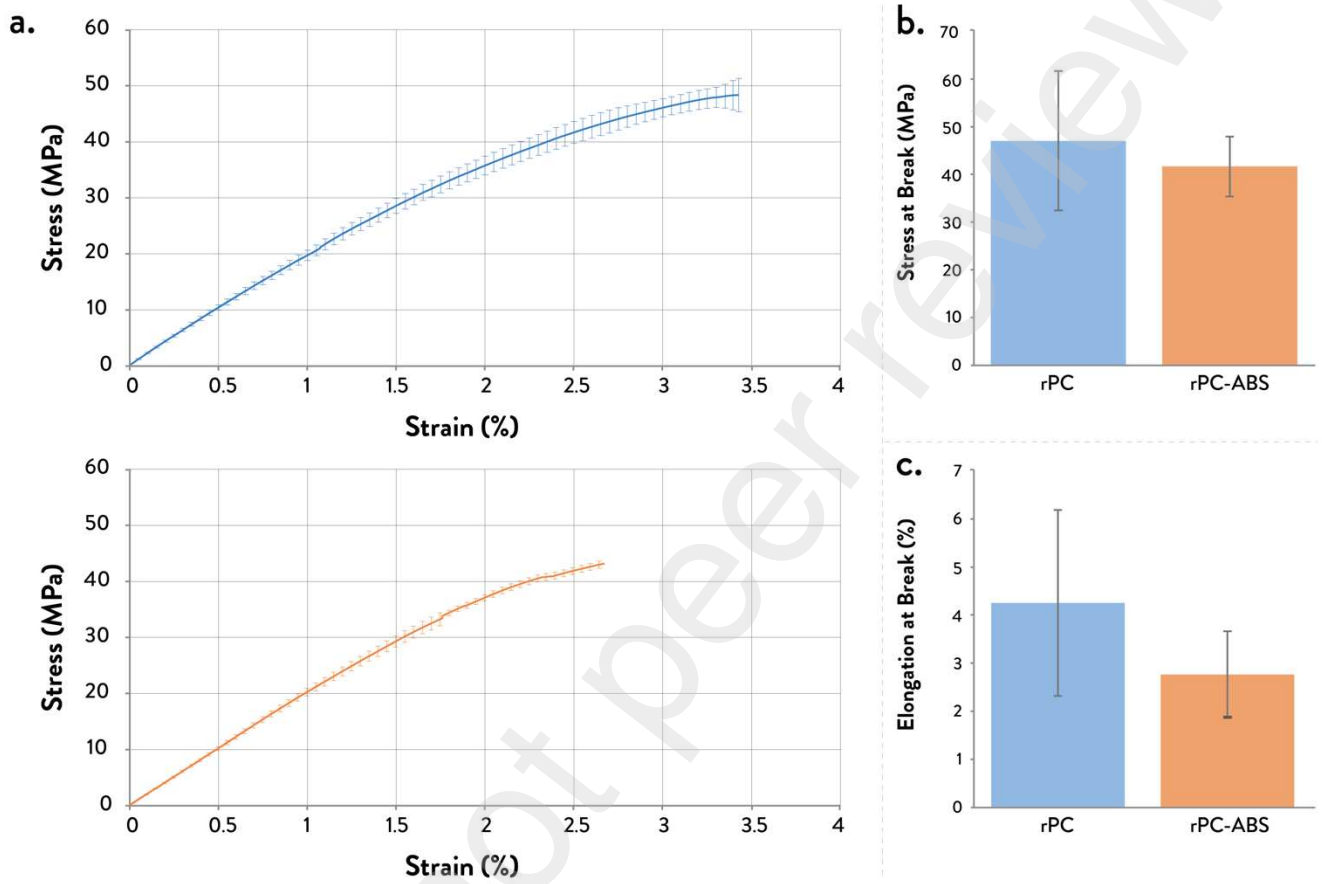

Fig. 7. Tensile tests: (a) mean stress-strain curves of 3-D printed recycled PC (top) and recycled PC/ABS (bottom); (b) stress at break and (c) elongation at break of recycled PC and recycled PC/ABS.

3.4 Impact tests

Samples for impact tests (Fig. 8a and b) confirmed the brittle failure mode of rPC and rPC/ABS formulations. The fracture surfaces showed almost no deformations or irregularities of the samples, maintaining their original rectangular cross-section shape. According to Table 5, Fig 8c and 8d, the impact resistance and impact energy of rPC/ABS remain comparable to rPC. The accuracy of the measurements for rPC/ABS increases, resulting in more reliable values. This fact may be linked to the use of 30% wt. of rABS pellet for the rPC/ABS formulation, decreasing the variability of recycled feedstock in terms of particle granulometry and shape. Accordingly, a consistent extrusion flow during the 3-D printing process results in fewer interlayer voids in the final part and the concomitant possible defects for cracking and premature failures.

Although Charpy tests may result in higher impact resistance and energy [90], lower values were obtained in previous studies with PC/ABS and FFF or FGF 3-D printing systems. For example, Verma and Banerjee reached ~15 kJ/m^2 of impact energy [91], whereas impact resistance values of ~350 J/m and ~200 J/m were obtained from Kumar et al. and Peng et al. [92,93]. The percentage of ABS can mainly influence these differences in PC/ABS blends characterized in these studies, i.e., 75% wt., and from the different scales of the 3-D printing process, mainly desktop-size small-format apparatuses. As a matter of fact, using FGF large-scale 3-D printers generally means using thicker layer heights and bigger nozzle diameters, causing over-extrusion trends during the process, longer cooling times, and bigger compressive deformations of the layers [88,78]. This

fact may help in reducing the dimension and frequency of cross-sectional interlayer voids, hence improving the fusion between layers and, consequently, the mechanical properties of the parts [91,64]. Furthermore, these values are comparable with virgin PC/ABS from injection molding. Chiu et al. reached impact energy values of ~90 kJ/m^2 for virgin PC/ABS [63], whereas Seo et al. obtained an impact resistance of ~150 J/m [57]. Although shape strongly influences the impact behavior of PC/ABS blends with high percentages of PC [57], results confirm a good interlayer adhesion of the samples, showing the potential of recycled feedstock and FGF systems in high-performance fields of application, i.e., technical equipment and sports.

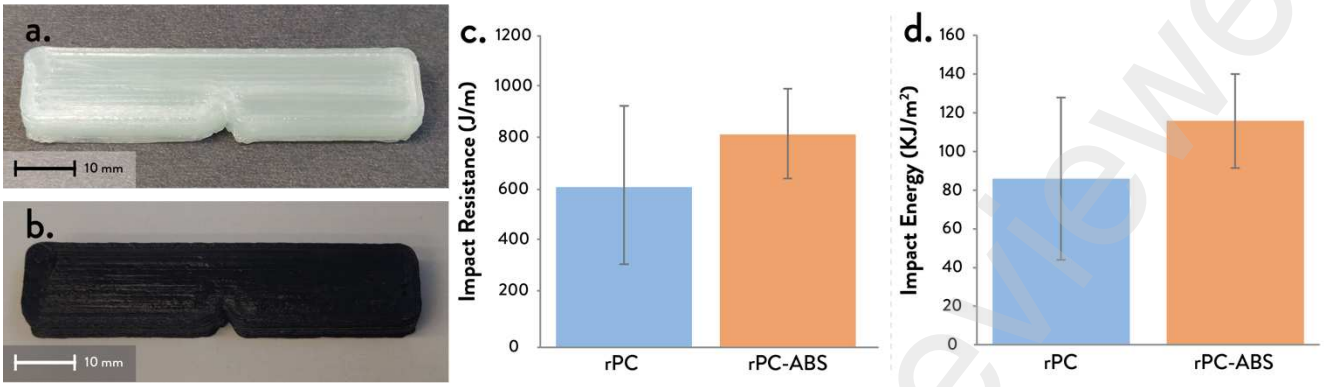

Fig. 8. Impact tests: specimens of (a) recycled PC and (b) recycled PC/ABS; (c) impact resistance and (d) impact energy of recycled PC and recycled PC/ABS.

Table 5. Experimental values from impact tests of 3-D printed recycled PC and recycled PC/ABS.

Material	**Neat Breaking Energy (J)**	**Impact Resistance *IR* (J/m)**	**Impact Energy *IE* (kJ/m²)**
Recycled PC	9 ± 4.45	609.66 ± 330.04	85.98 ± 42.02
Recycled PC/ABS	11.43 ± 2.15	810.36 ± 165.77	115.78 ± 24.40

3.5 Fracture analysis

Micrograph images on the fracture cross-section surfaces were made to evaluate the 3-D printing quality of the tested materials. In general, 3-D printed paths are less noticeable than those observed in FFF systems [60,61]. In the case of rPC (Fig. 9a), the fracture surface is quite homogeneous without visible voids in the cross-section. The direction of the brittle fracture is visible thanks to the whitened cracks close to the notch, which means on the left side of the cross-section. Moreover, few marks from the 3-D printing process are visible, i.e., division of the extrusion paths. This confirms the good quality of the extrusion flow and its homogeneous consistency, also influenced by the over-extrusion noticed in the comparison tests of Section 3.1. As a result, some over-extrusion may help in improving the interlayer adhesion by reducing the presence of voids typical of the FFF and FGF processes, achieving higher mechanical properties [64].

For the rPC/ABS samples (Fig. 9b), more visible voids can be seen in the cross-section of the samples. The direction of the fracture is not clearly noticeable, and only some cracks can be seen close to the notch. Considering the 3-D printing process, the extrusion path is quite noticeable in some points, i.e., the external perimeter of the sample on the right side, as well as the different layers and the building orientation of the sample. This fact can result from the reduced over-extrusion compared to rPC, although some points show better interlayer adhesion, i.e., the right bottom corner of the cross-section. In short, consistent extrusion lines can be reached with both materials, especially with rPC, and tuning the 3-D printing parameters related to the extrusion flow may help in obtaining parts with higher bonding and fewer voids.

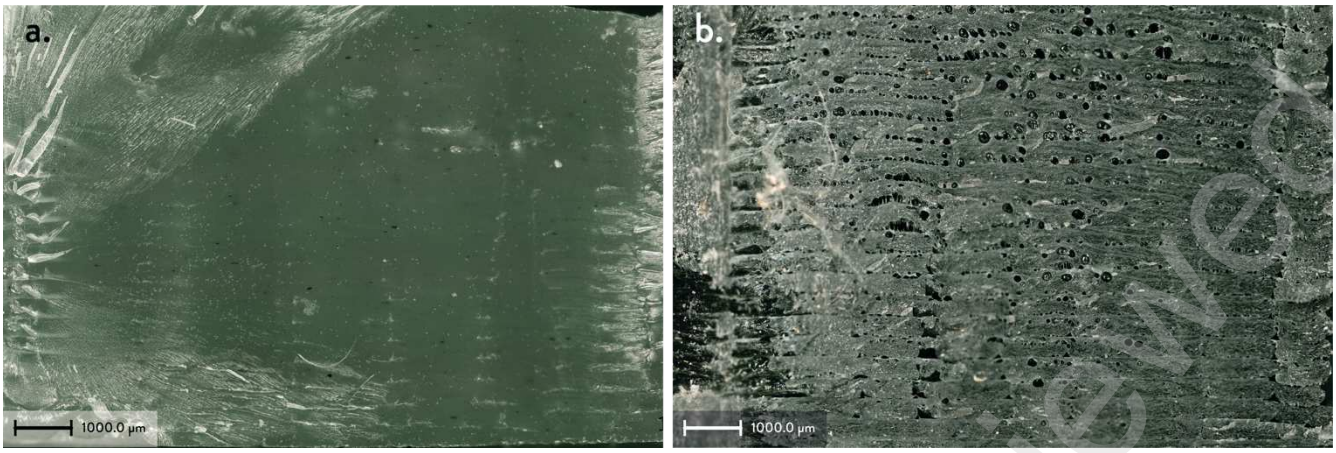

Fig. 9. Microscope micrographs of the fracture cross-sections from the impact test: (a) recycled PC and (b) recycled PC/ABS (100 x magnification).

3.6 Fostering new product applications: case studies

After the previous characterization tests, some plausible application case studies were analyzed to demonstrate the use of rPC and rPC/ABS for real applications, aiming to reduce the gap between experimental studies and exploitation in real contexts. The literature indicates that AM technologies show great potential in fostering sustainable and circular design practices in practical contexts, i.e., in industrial contexts or design projects [94,23]. Furthermore, a growing number of projects and initiatives have been focusing on using recycled materials for new products, demonstrating an interest in exploring new applications and paths toward sustainable models of production and consumption [95,96]. As summarized in Table 6, some real applications were found in the last five years considering recycled PC or recycled ABS and FFF/FGF processes. In most cases, the application field is related to technical equipment [11,55] or furniture elements [97,98], dealing both with small and large-scale 3-D printing systems. No real applications, however, were found with recycled PC/ABS blends, although these materials offer good mechanical and technical properties to be exploited in new products, especially for high-performance applications that require better processability, thermal stability, or good impact resistance [60,99]. Considering the results achieved in this work, customized protective sports equipment represents a good case study for the exploitation of recycled PC/ABS blends for FGF systems.

Table 6. Resume of the main application-driven works and design projects dealing with FFF or FGF 3-D printing of PC and ABS adapted from [96].

Material	Source	Year	3-D printing system	Application fields and products
rPC/ABS	//	//	//	No applications found
rPC	[55]	2019	Large-format FGF (GigabotX)	Household appliances and tooling - Molds, part replacement, car accessories
	[97]	2018	Large-format FFF	Furniture – indoor cabinet
rABS	[100]	2018	Small-format FFF	Gardening – Piping connectors
	[11]	2018	Small-format FFF	Photography equipment – Camera tripod and hood
	[43]	2019	Large-format FGF	Sporting goods – Skateboard, kayak paddle, snowshoes
	[98]	2020	Small-format FFF	Urban furniture – outdoor modules
	[101]	2022	Small-format FFF	Medical technology – Patient sensor

Protective shin guards and customizable furniture elements were selected as a proof-of-concept to be designed and fabricated with rPC/ABS and GigabotX. The first demo product (Fig. 10a) is made of a main external structural part in rPC/ABS combined with a flexible internal shape made of thermoplastic polyurethane (TPU). The two parts can be customized according to the user by modifying their overall dimensions and pattern, i.e., the pattern fill percentage, adapting the technical properties of the product according to the use and the specific sport activity.

Focusing on rPC/ABS, the external structure was designed to be 3-D printed as a flat component to reduce material waste during the fabrication and printing times. The overall geometry was developed by considering the possible extrusion path of the 3-D printing hot end, as visible in the gcode preview of Fig. 10b. After its fabrication, the external structural part can be easily adapted with an accessible heat source, i.e., a hot gun that can be used to seal pores [102] and reshape, to reach the 3-D profile of legs and ankles. The demo shin guard was designed by following these key principles [103, 104]:

- The pattern was created by defining a single curve, representing the path followed by the extrusion hot end, limiting the travel paths to be done, hence retraction-related issues with bigger nozzles.
- A longer path was created to allow each layer to cool down properly before the following layer, especially in case of over-extrusion and/or thicker layer heights.
- Printing a flat customized component helps in reducing the printing times and waste of material, i.e., for support generation, and in improving the adhesion of the whole part by increasing the area touching the build plate.
- The thickness of the pattern is influenced by the nozzle dimension, which also was considered a variable in customizing the shape of the final design.

Fig. 10c shows the 3-D printed part, whereas the result after manual thermoforming is visible in Fig. 10d. The overall 3-D printing quality was satisfactory from a functional point of view, although the part required post-processing to remove some exceeding material, i.e., from stringing. This result validates the potential use of rPC/ABS and FGF systems with complex layer patterns for customizable technical applications, such as in the sports goods sector (Fig. 10e).

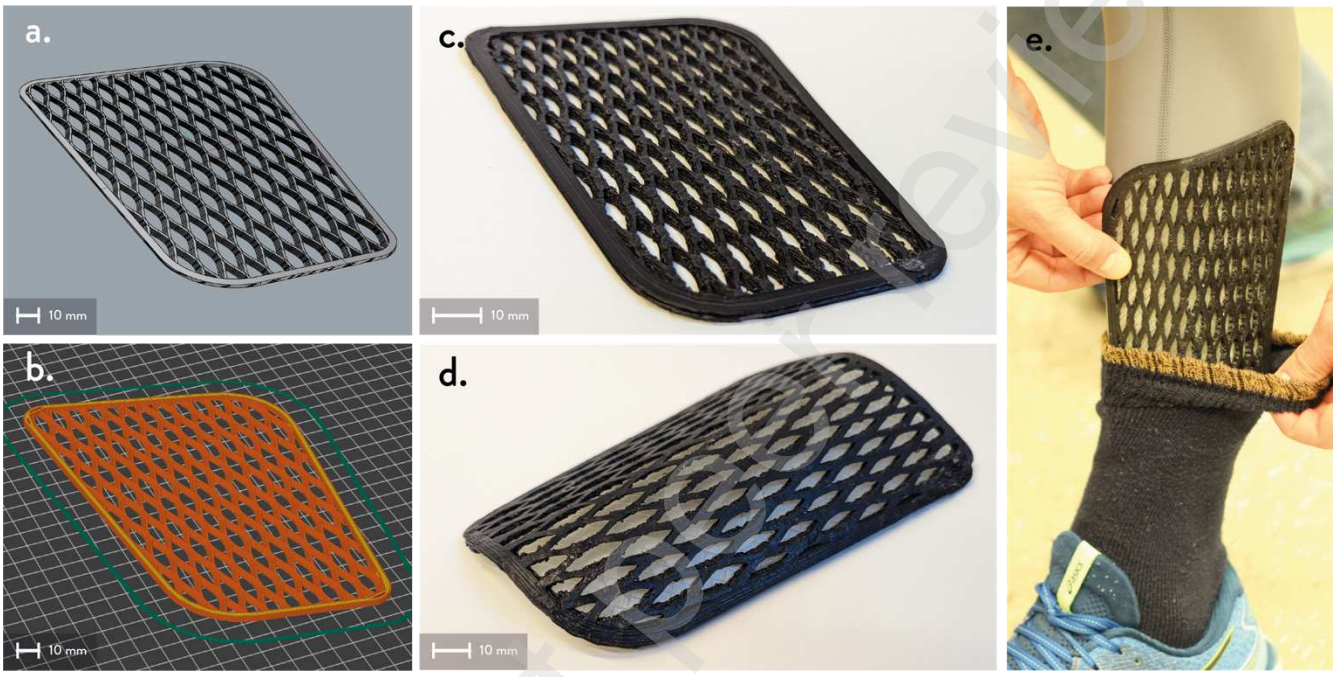

Fig. 10. Application case study from sporting goods sector (protective equipment – shin-guard): (a) 3-D model; (b) gcode preview; (c) 3-D printed part (flat design); (d) 3-D printed part after manual thermoforming; (e) result showing athlete preparing for soccer (football) match.

Further validation comes from the 3-D printing of a second demo product from the furniture sector. The selected 3-D model is a joint for a customizable coat hanger rack and can be used to evaluate the potentials and limitations of GigabotX in terms of achievable features and shapes [54]. Fig. 12a shows the gcode preview of the part sliced with a printing speed of 40 mm/s, according to the results from the first printing test (Section 3.1). Hence, the part can be obtained in less than 1h 30m, allowing fast replication of customized joints. The result is visible in Fig. 12b, which validates the use of recycled PC/ABS feedstock to fabricate more complex 3-D shapes, i.e., furniture elements. The main features of the model were successfully achieved, i.e., incremental overhangs, different cross-section shapes, and assembly tolerances. Moreover, no deformation or delamination was detected in the 3-D printed part. In general, the quality of the 3-D printed parts can be compared to other commercial FGF systems or virgin material feedstock, showing the potential of using recycled materials for new applications in DRAM contexts. Furthermore, the achieved quality can help in facilitating the acceptance of recycled polymers for the end-users, reducing the gap between virgin and recycled feedstock in terms of perceived quality for accessible products [105-107].

The next step in future work can consider the design and production of large-scale components, i.e., large-size furniture elements, or more complex geometries for technical applications, i.e., freeform customized protective helmets, elbow protectors, full-scale 3-D printed furniture, and automotive components [108]. Moreover, similar application fields may use digital imaging technologies to customize the final design, i.e., photogrammetry or x-ray imaging, taking advantage of distributed AM of high-performance recycled feedstock.

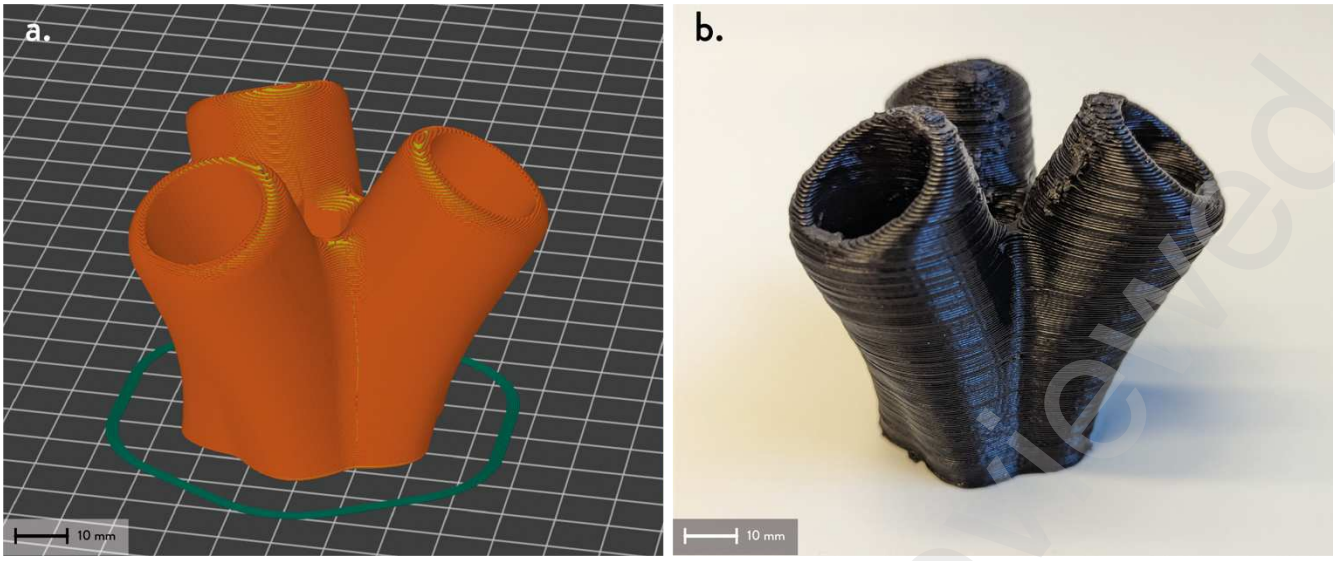

Fig. 12. Application case study from furniture sector (coat hanger joint) [54]: (a) gcode preview and (b) 3-D printed part.

4. Conclusions

This work demonstrated the potential of using recycled PC/ABS feedstock with large-format FGF 3-D printing systems. After modifying a commercial open source FGF 3-D printer, the accuracy and printability of the two feedstocks were assessed with 3-D printed samples. Tensile and impact tests were performed to better understand the mechanical behavior of 3-D printed specimens, as well as to analyze their fracture surfaces. The influence of weather on the samples was assessed through a weather simulation test. The feasibility of using recycled feedstock for real applications was finally evaluated by choosing two application fields and fabricating two different demo products, i.e., customizable protective shin guards and furniture joints.

In general, better printability was achieved with recycled PC/ABS compared to recycled PC, as well as good dimensional accuracy, especially at 30 and 40 mm/s. These results demonstrate the influence of rABS pellets in improving the printability of recycled PC shard-based feedstock. Minimal qualitative differences and discoloration were visible on the samples after accelerated weather exposure of 24h, with results in accordance with the state-of-the-art. These results indicate the materials may be used for outdoor applications. The results from tensile tests show similar values of elastic modulus, tensile strength, and elongation at break for rPC and rPC/ABS, comparable with previously studied virgin 3-D printed filaments. Similarly, impact energy and resistance values are comparable in the two tested formulations, reaching similar results compared to FFF 3-D printed filaments, as well as virgin materials for injection molding. Although some voids and interlayer gaps are visible from the fracture surfaces, these results confirm the possible use of rPC and rPC/ABS in functional applications. Finally, the two demonstration products in the sporting goods and furniture sectors were successfully fabricated with rPC/ABS, achieving complex patterns and good printing speeds for recycled feedstocks.

In summary, rPC/ABS blends represent a potential high-performance feedstock for DRAM, validating its use in direct FGF 3-D printing systems. In addition, new application fields can be capitalized on in circular economy contexts following DRAM principles, including technical sectors. Further research is needed in future work to assess the mechanical properties of 3-D printed rPC/ABS blends, such as flexural and bending tests, and other characterizations can be performed to deepen the knowledge of these blends, i.e., other percent mixtures and thermal characterization. Future work should also focus on larger and more complex parts to fabricate while also considering a broader range of application fields. Finally, full environmental and economic life cycle analyses should be run on this new recycled blend material applications of DRAM.

Acknowledgements

The authors would thank Aliaksei Petsiuk for the technical support. This study was supported by the Thompson Endowments and the Natural Sciences and Engineering Research Council of Canada.

References

1. Kosior E, Crescenzi I. Solutions to the plastic waste problem on land and in the oceans. In Plastic waste and recycling 2020 Jan 1, pp. 415-446. Academic Press.

2. Faludi J, Cline-Thomas N, Agrawala S. 3D printing and its environmental implications. In: The Next Production Revolution: Implications for Governments and Business, OECD Publishing, 2017, Paris, France, ch. 5, pp. 171-213. https://doi.org/10.1787/9789264271036-en.
3. Jones, R., Haufe, P., Sells, E., Iravani, P., Olliver, V., Palmer, C., & Bowyer, A. (2011). RepRap–the replicating rapid prototyper. Robotica, 29(1), 177-191.
4. Sells, E., Bailard, S., Smith, Z., Bowyer, A., & Olliver, V. (2010). RepRap: the replicating rapid prototyper: maximizing customizability by breeding the means of production. In Handbook of Research in Mass Customization and Personalization: (In 2 Volumes) (pp. 568-580).
5. Bowyer A. 3D printing and humanity's first imperfect replicator. 3D printing and additive manufacturing 2014, 1(1), 4-5.
6. Hoy, M. B. (2013). 3D printing: making things at the library. Medical reference services quarterly, 32(1), 93-99.
7. De Jong, J.P. and De Bruijn, E., 2012. Innovation lessons from 3-D printing. MIT Sloan Management Review.
8. Nilsiam, Y., & Pearce, J. M. (2017). Free and open source 3-D model customizer for websites to democratize design with OpenSCAD. Designs, 1(1), 5.
9. Barrett A. Is PLA Recyclable? 2020. https://bioplasticsnews.com/2020/04/05/is-pla-recyclable. (accessed 08 March 2023).
10. Globe Newswire. The Market for Additive Manufacturing in the Oil and Gas Sector 2018-2029. 2019. https://www.globenewswire.com/news-release/2019/06/04/1864243/0/en/NewSmarTech-Analysis-Report-on-Additive-Manufacturing-in-the-Oil-and-Gas-IndustryFinds-1B-Opportunity-for-AM-Hardware-Manufacturers.html. (accessed 08 March 2023).
11. Zhong S, Pearce JM. Tightening the loop on the circular economy: Coupled distributed recycling and manufacturing with recyclebot and RepRap 3-D printing. Resour. Conserv. Recycl. 2018. 128, 48–58. https://doi.org/10.1016/j.resconrec.2017.09.023.
12. Santander P, Sanchez FAC, Boudaoud H, & Camargo M. Closed loop supply chain network for local and distributed plastic recycling for 3D printing: a MILP-based optimization approach. Resour. Conserv. Recycl. 2020, 154, 104531.
13. Sanchez FAC, Boudaoud H, Camargo M, Pearce JM. Plastic recycling in additive manufacturing: A systematic literature review and opportunities for the circular economy. J. Clean. Prod. 2020, 264, 121602. https://doi.org/10.1016/j.jclepro.2020.121602.
14. Pavlo S, Fabio C, Hakim B, Mauricio C. 3D-Printing Based Distributed Plastic Recycling: A Conceptual Model for Closed-Loop Supply Chain Design. In Proceedings of the 2018 IEEE International Conference on Engineering, Technology and Innovation (ICE/ITMC), 2018, Stuttgart, Germany, pp. 1–8.
15. Dertinger SC, Gallup N, Tanikella NG et al. Technical pathways for distributed recycling of polymer composites for distributed manufacturing: Windshield wiper blades. Resour. Conserv. Recycl. 2020, 157, 104810.
16. Kreiger MA, Mulder ML, Glover AG, & Pearce JM. Life cycle analysis of distributed recycling of post-consumer high density polyethylene for 3-D printing filament. J. Clean. Prod. 2014, 70, 90-96.
17. Kreiger M & Pearce JM. Environmental life cycle analysis of distributed three-dimensional printing and conventional manufacturing of polymer products. ACS Sustainable Chemistry & Engineering 2013, 1(12), 1511-1519.
18. Gwamuri J, Wittbrodt BT, Anzalone NC & Pearce JM. Reversing the trend of large scale and centralization in manufacturing: The case of distributed manufacturing of customizable 3-D-printable self-adjustable glasses. Challenges in Sustainability 2014, 2(1), 30-40. DOI: 10.12924/cis2014.02010030.
19. Wittbrodt, B. T., Glover, A. G., Laureto, J., Anzalone, G. C., Oppliger, D., Irwin, J. L., & Pearce, J. M. (2013). Life-cycle economic analysis of distributed manufacturing with open-source 3-D printers. Mechatronics, 23(6), 713-726.
20. Pearce, J., & Qian, J. Y. (2022). Economic Impact of Home Manufacturing of Consumer Products with Low-cost 3D Printing of Free and Open-Source Designs. European Journal of Social Impact and Circular Economy-ISSN, 2704, 9906.
21. Petersen EE & Pearce JM. Emergence of home manufacturing in the developed world: Return on investment for open-source 3-D printers. Technologies 2017, 5(1), 7. https://doi.org/10.3390/technologies5010007
22. Mohammed M, Wilson D, Gomez-Kervin E et al. Sustainability and feasibility assessment of distributed E-waste recycling using additive manufacturing in a Bi-continental context. Additive Manufacturing 2022, 50, 102548. https://doi.org/10.1016/j.addma.2021.102548.
23. Laplume AO, Petersen B, Pearce JM. Global value chains from a 3D printing perspective. J. Int. Bus. Stud. 2016, 47, 595–609. https://doi.org/10.1057/jibs.2015.47.
24. Zhong S, Rakhe P & Pearce JM. Energy payback time of a solar photovoltaic powered waste plastic recyclebot system. Recycling 2017, 2(2), 10.
25. Woern AL, McCaslin JR, Pringle AM, Pearce JM. RepRapable Recyclebot: Open source 3-D printable extruder for converting plastic to 3-D printing filament. HardwareX 2018, 4, e00026, https://doi.org/10.1016/j.ohx.2018.e00026.
26. Cress AK, Huynh J, Anderson EH, O'neill R, Schneider Y, Keleş Ö. Effect of recycling on the mechanical behavior and structure of additively manufactured acrylonitrile butadiene styrene (ABS). Journal of Cleaner Production 2021;279:123689. https://doi.org/10.1016/j.jclepro.2020.123689.
27. Mohammed MI, Wilson D, Gomez-Kervin E, Tang B, Wang J. Investigation of Closed-Loop Manufacturing with Acrylonitrile Butadiene Styrene over Multiple Generations Using Additive Manufacturing. ACS Sustainable Chem Eng

2019;7:13955–69. https://doi.org/10.1021/acssuschemeng.9b02368.
28. Vidakis N, Petousis M, Maniadi A, Koudoumas E, Vairis A, Kechagias J. Sustainable Additive Manufacturing: Mechanical Response of Acrylonitrile-Butadiene-Styrene over Multiple Recycling Processes. Sustainability 2020;12:3568. https://doi.org/10.3390/su12093568.
29. Mohammed MI, Wilson D, Gomez-Kervin E, Rosson L, Long J. EcoPrinting: Investigation of Solar Powered Plastic Recycling and Additive Manufacturing for Enhanced Waste Management and Sustainable Manufacturing. 2018 IEEE Conference on Technologies for Sustainability (SusTech), 2018, p. 1–6. https://doi.org/10.1109/SusTech.2018.8671370.
30. Anderson I. Mechanical Properties of Specimens 3D Printed with Virgin and Recycled Polylactic Acid. 3D Printing and Additive Manufacturing 2017;4:110–5. https://doi.org/10.1089/3dp.2016.0054.
31. Baechler C, DeVuono M, Pearce JM. Distributed recycling of waste polymer into RepRap feedstock. Rapid Prototyping Journal 2013;19:118–25. https://doi.org/10.1108/13552541311302978.
32. Chong S, Pan G-T, Khalid M, Yang TC-K, Hung S-T, Huang C-M. Physical Characterization and Pre-assessment of Recycled High-Density Polyethylene as 3D Printing Material. J Polym Environ 2017;25:136–45. https://doi.org/10.1007/s10924-016-0793-4.
33. Zander NE, Gillan M, Lambeth RH. Recycled polyethylene terephthalate as a new FFF feedstock material. Additive Manufacturing 2018;21:174–82. https://doi.org/10.1016/j.addma.2018.03.007.
34. Sanchez FAC, Boudaoud H, Hoppe S, Camargo M. Polymer recycling in an open-source additive manufacturing context: Mechanical issues. Additive Manufacturing 2017;17:87–105. https://doi.org/10.1016/j.addma.2017.05.013.
35. Laoutid F, Lafqir S, Toncheva A, Dubois P. Valorization of Recycled Tire Rubber for 3D Printing of ABS- and TPO-Based Composites. Materials 2021;14:5889. https://doi.org/10.3390/ma14195889.
36. Maldonado-García B, Pal AK, Misra M, Gregori S, Mohanty AK. Sustainable 3D printed composites from recycled ocean plastics and pyrolyzed soy-hulls: Optimization of printing parameters, performance studies and prototypes development. Composites Part C: Open Access 2021;6:100197. https://doi.org/10.1016/j.jcomc.2021.100197.
37. Martey S, Hendren K, Farfaras N, Kelly JC, Newsome M, Ciesielska-Wrobel I, et al. Recycling of Pretreated Polyolefin-Based Ocean-Bound Plastic Waste by Incorporating Clay and Rubber. Recycling 2022;7:25. https://doi.org/10.3390/recycling7020025.
38. Zander NE, Gillan M, Burckhard Z, Gardea F. Recycled polypropylene blends as novel 3D printing materials. Additive Manufacturing 2019;25:122–30. https://doi.org/10.1016/j.addma.2018.11.009.
39. Woern AL, Byard DJ, Oakley RB et al. Fused particle fabrication 3-D printing: Recycled materials' optimization and mechanical properties. Materials 2018, 11(8), 1413. https://doi.org/10.3390/ma11081413.
40. Little HA, Tanikella NG, Reich MJ et al. Towards distributed recycling with additive manufacturing of PET flake feedstocks. Materials 2020, 13(19), 4273.
41. Whyman S, Arif KM & Potgieter J. Design and development of an extrusion system for 3D printing biopolymer pellets. The International Journal of Advanced Manufacturing Technology 2018, 96(9), 3417-3428.
42. Alexandre A, Sanchez FAC, Boudaoud H et al. Mechanical properties of direct waste printing of polylactic acid with universal pellets extruder: comparison to fused filament fabrication on open-source desktop three-dimensional printers. 3D Printing and Additive Manufacturing 2020, 7(5), 237-247.
43. Byard DJ, Woern AL, Oakley RB et al. Green fab lab applications of large-area waste polymer-based additive manufacturing. Additive Manufacturing 2019, 27, 515-525.
44. Gigabot XLT (re3d), https://re3d.org/portfolio/gigabot-xlt.
45. Exabot (re3d), https://re3d.org/portfolio/exabot.
46. Terabot (re3d), https://re3d.org/portfolio/terabot.
47. THE BOX Large (BLB Industries), https://www.aniwaa.com/product/3d-printers/blb-industries-the-box-large.
48. T3500 (Tractus3D), https://www.aniwaa.com/product/3d-printers/tractus3d-t3500-rtp.
49. 400 Series WORKBENCH XTREME (3D Platform), https://www.aniwaa.com/product/3d-printers/3d-platform-400-series-workbench-xtreme.
50. BIG-Meter (Modix), https://www.aniwaa.com/product/3d-printers/modix-big-meter.
51. BigRep ONE v4 (BigRep), https://www.aniwaa.com/product/3d-printers/bigrep-one.
52. F1000 (CreatBot), https://www.aniwaa.com/product/3d-printers/creatbot-f1000.
53. Petsiuk, A., Lavu, B., Dick, R., & Pearce, J. M. (2022). Waste Plastic Direct Extrusion Hangprinter. Inventions, 7(3), 70
54. Rattan RS, Nauta N, Romani A, Pearce JM. Hangprinter for large scale additive manufacturing using fused particle fabrication with recycled plastic and continuous feeding. HardwareX 2023;13:e00401. https://doi.org/10.1016/j.ohx.2023.e00401.
55. Reich MJ, Woern AL, Tanikella NG & Pearce JM. Mechanical properties and applications of recycled polycarbonate particle material extrusion-based additive manufacturing. Materials 2019, 12(10), 1642.
56. Akkapeddi MK. Commercial Polymer Blends. In: Utracki LA, editor. Polymer Blends Handbook, Dordrecht: Springer Netherlands; 2003, p. 1023–115. https://doi.org/10.1007/0-306-48244-4_15.
57. Seo JS, Jeon HT, Han TH. Effects of blend composition on the morphologies and physical properties of polycarbonate/acrylonitrile-butadiene-styrene blends. Journal of Applied Polymer Science 2021;138:50404. https://doi.org/10.1002/app.50404.

58. Krache R, Debah I. Some Mechanical and Thermal Properties of PC/ABS Blends. Materials Sciences and Applications 2011;02:404. https://doi.org/10.4236/msa.2011.25052.
59. PC-ABS: Polycarbonate Material Properties. https://www.xometry.com/resources/materials/pc-abs/ (accessed March 22, 2023).
60. Kannan S, Ramamoorthy M. Mechanical characterization and experimental modal analysis of 3D Printed ABS, PC, and PC-ABS materials. Mater Res Express 2020;7:015341. https://doi.org/10.1088/2053-1591/ab6a48.
61. Yap YL, Toh W, Koneru R, Lin K, Yeoh KM, Lim CM, et al. A non-destructive experimental-cum-numerical methodology for the characterization of 3D-printed materials—polycarbonate-acrylonitrile butadiene styrene (PC-ABS). Mechanics of Materials 2019;132:121–33. https://doi.org/10.1016/j.mechmat.2019.03.005.
62. Rivet I, Dialami N, Cervera M, Chiumenti M, Reyes G, Pérez MA. Experimental, Computational, and Dimensional Analysis of the Mechanical Performance of Fused Filament Fabrication Parts. Polymers 2021;13:1766. https://doi.org/10.3390/polym13111766.
63. Chiu H-T, Huang J-K, Kuo M-T, Huang J-H. Characterisation of PC/ABS blend during 20 reprocessing cycles and subsequent functionality recovery by virgin additives. Journal of Polymer Research 2018;25. https://doi.org/10.1007/s10965-018-1522-6.
64. Zhou Y-G, Zou J-R, Wu H-H, Xu B-P. Balance between bonding and deposition during fused deposition modeling of polycarbonate and acrylonitrile-butadiene-styrene composites. Polymer Composites 2020;41:60–72. https://doi.org/10.1002/pc.25345.
65. Mohamed OA, Masood SH, Bhowmik JL, Nikzad M, Azadmanjiri J. Effect of Process Parameters on Dynamic Mechanical Performance of FDM PC/ABS Printed Parts Through Design of Experiment. J of Materi Eng and Perform 2016;25:2922–35. https://doi.org/10.1007/s11665-016-2157-6.
66. PrusaSlicer releases (Github), https://github.com/prusa3d/PrusaSlicer/releases (accessed Apr 4, 2023).
67. Pearce, JM, Romani. A. Designs for Recycled PC and PC-ABS feedstock project, Feb. 2023, Accessed: April. 6, 2023. [Online]. https://osf.io/z9fnk/
68. ASTM D5071-06. Standard Practice for Exposure of Photodegradable Plastics in a Xenon Arc Apparatus, 2021.
69. ASTM D2244-22. Standard Practice for Calculation of Color Tolerances and Color Differences from Instrumentally Measured Color Coordinates, 2022.
70. ASTM D638-22. Standard Test Method for Tensile Properties of Plastics, 2022.
71. Laureto JJ, Pearce JM. Anisotropic mechanical property variance between ASTM D638-14 type i and type iv fused filament fabricated specimens. Polymer Testing 2018;68:294–301. https://doi.org/10.1016/j.polymertesting.2018.04.029.
72. Dizon JRC, Espera AH, Chen Q, Advincula RC. Mechanical characterization of 3D-printed polymers. Additive Manufacturing 2018;20:44–67. https://doi.org/10.1016/j.addma.2017.12.002.
73. ASTM D6110-18. Standard Test Method for Determining the Charpy Impact Resistance of Notched Specimens of Plastics, 2018.
74. Marlin. Marlin Firmware - Fabricating Fused Filament. Marlin Firmware 2011. https://marlinfw.org/ (accessed February 2, 2023).
75. Nieto DM, Molina SI. Large-format fused deposition additive manufacturing: a review. Rapid Prototyp J 2019. https://doi.org/10.1108/RPJ-05-2018-0126.
76. Akbaş OE, Hıra O, Hervan SZ, Samankan S, Altınkaynak A. Dimensional accuracy of FDM-printed polymer parts. Rapid Prototyping Journal 2019;26:288–98. https://doi.org/10.1108/RPJ-04-2019-0115.
77. Agarwal KM, Shubham P, Bhatia D, Sharma P, Vaid H, Vajpeyi R. Analyzing the Impact of Print Parameters on Dimensional Variation of ABS specimens printed using Fused Deposition Modelling (FDM). Sensors International 2022;3:100149. https://doi.org/10.1016/j.sintl.2021.100149.
78. Meraz Trejo E, Jimenez X, Billah KMM, Seppala J, Wicker R, Espalin D. Compressive deformation analysis of large area pellet-fed material extrusion 3D printed parts in relation to in situ thermal imaging. Additive Manufacturing 2020;33:101099. https://doi.org/10.1016/j.addma.2020.101099.
79. Choo K, Friedrich B, Daugherty T, Schmidt A, Patterson C, Abraham MA, et al. Heat retention modeling of large area additive manufacturing. Additive Manufacturing 2019;28:325–32. https://doi.org/10.1016/j.addma.2019.04.014.
80. Mbow MM, Marin PR, Pourroy F. Extruded diameter dependence on temperature and velocity in the fused deposition modeling process. Prog Addit Manuf 2020;5:139–52. https://doi.org/10.1007/s40964-019-00107-4.
81. Babbar I, Mathur GN. Rheological properties of blends of polycarbonate with poly(acrylonitrile-butadiene-styrene). Polymer 1994;35:2631–5. https://doi.org/10.1016/0032-3861(94)90391-3.
82. Al Harraq A, Brahana PJ, Arcemont O, Zhang D, Valsaraj KT, Bharti B. Effects of Weathering on Microplastic Dispersibility and Pollutant Uptake Capacity. ACS Environ 2022;2:549–55. https://doi.org/10.1021/acsenvironau.2c00036.
83. Santos RM, Botelho GL, Cramez C, Machado AV. Outdoor and accelerated weathering of acrylonitrile-butadiene-styrene: A correlation study. Polymer Degradation and Stability 2013;98:2111–5. https://doi.org/10.1016/j.polymdegradstab.2013.07.016.
84. Pickett JE, Gibson DA, Gardner MM. Effects of irradiation conditions on the weathering of engineering thermoplastics. Polymer Degradation and Stability 2008;93:1597–606. https://doi.org/10.1016/j.polymdegradstab.2008.02.009.
85. Signoret C, Edo M, Lafon D, Caro-Bretelle A-S, Lopez-Cuesta J-M, Ienny P, et al. Degradation of Styrenic Plastics

During Recycling: Impact of Reprocessing Photodegraded Material on Aspect and Mechanical Properties. J Polym Environ 2020;28:2055–77. https://doi.org/10.1007/s10924-020-01741-8.
86. Wee J-W, Choi M-S, Hyun H-C, Hwang J-H, Choi B-H. Observation and Modeling of the Effects of Temperature and UV Lights on Weathering-Induced Degradation of PC/ABS Blend for Sustainable Consumer Electronics. Int J of Precis Eng and Manuf-Green Tech 2022;9:1369–85. https://doi.org/10.1007/s40684-021-00392-x.
87. Yildirim FF, Sezer Hicyilmaz A, Yildirim K. The effects of the weathering methods on the properties of the ABS, ASA and PMMA polymers. Polymer Testing 2022;107:107484. https://doi.org/10.1016/j.polymertesting.2022.107484.
88. D'Amico T, Peterson AM. Bead parameterization of desktop and room-scale material extrusion additive manufacturing: How print speed and thermal properties affect heat transfer. Additive Manufacturing 2020;34:101239. https://doi.org/10.1016/j.addma.2020.101239.
89. Orzan E, Janewithayapun R, Gutkin R, Lo Re G, Kallio K. Thermo-mechanical variability of post-industrial and post-consumer recyclate PC-ABS. Polymer Testing 2021;99:107216. https://doi.org/10.1016/j.polymertesting.2021.107216.
90. Tanveer MdQ, Haleem A, Suhaib M. Effect of variable infill density on mechanical behaviour of 3-D printed PLA specimen: an experimental investigation. SN Appl Sci 2019;1:1701. https://doi.org/10.1007/s42452-019-1744-1
91. Verma N, S A, Banerjee SS. Development of material extrusion 3D printable ABS/PC polymer blends: influence of styrene–isoprene–styrene copolymer on printability and mechanical properties. Polymer-Plastics Technology and Materials. 2022;1–14. https://doi.org/10.1080/25740881.2022.2121218
92. Kumar M, Ramakrishnan R, Omarbekova A. 3D printed polycarbonate reinforced acrylonitrile–butadiene–styrene composites: Composition effects on mechanical properties, micro-structure and void formation study. J Mech Sci Technol 2019;33:5219–26. https://doi.org/10.1007/s12206-019-1011-9.
93. Peng F, Jiang H, Woods A, Joo P, Amis EJ, Zacharia NS, et al. 3D Printing with Core–Shell Filaments Containing High or Low Density Polyethylene Shells. ACS Appl Polym Mater 2019;1:275–85. https://doi.org/10.1021/acsapm.8b00186.
94. Sauerwein M, Doubrovski E, Balkenende R, Bakker C. Exploring the potential of additive manufacturing for product design in a circular economy. J Clean Prod 2019;226:1138–49. https://doi.org/10.1016/j.jclepro.2019.04.108.
95. Mikula K, Skrzypczak D, Izydorczyk G, Warchoł J, Moustakas K, Chojnacka K, et al. 3D printing filament as a second life of waste plastics—a review. Environ Sci Pollut Res 2021;28:12321–33. https://doi.org/10.1007/s11356-020-10657-8.
96. Romani A, Rognoli V, Levi M. Design, Materials, and Extrusion-Based Additive Manufacturing in Circular Economy Contexts: From Waste to New Products. Sustainability 2021;13:7269. https://doi.org/10.3390/su13137269.
97. "Not only hollow" cabinet: Adorno Design. Adorno 2018. https://adorno.design/pieces/not-only-hollow-cabinet/ (accessed February 9, 2021).
98. Esirger SB, Örnek MA. Recycled Plastic to Performative Urban Furniture. J Digit Landsc Archit 2020:166–72. https://doi.org/10.14627/537690018
99. Kumar P, Gupta P, Singh I. Performance Analysis of Acrylonitrile–Butadiene–Styrene–Polycarbonate Polymer Blend Filament for Fused Deposition Modeling Printing Using Hybrid Artificial Intelligence Algorithms. J of Materi Eng and Perform 2022. https://doi.org/10.1007/s11665-022-07243-z.
100. Mohammed MI, Wilson D, Gomez-Kervin E, Vidler C, Rosson L, Long J. The recycling of E-Waste ABS plastics by melt extrusion and 3D printing using solar powered devices as a transformative tool for humanitarian aid. SFF 2018 : Proceedings of the 29th Annual International Solid Freeform Fabrication Symposium - An Additive Manufacturing Conference, University of Texas, Austin: 2018, p. 14.
101. Jain C, Dhaliwal BS, Singh R, Kumar V. Investigations on 3D printed primary recycled ABS for one-way programming. Advances in Materials and Processing Technologies 2022;0:1–14. https://doi.org/10.1080/2374068X.2022.2109641.
102. Mayville PJ, Petsiuk AL, Pearce J.M. Thermal Post-Processing of 3D Printed Polypropylene Parts for Vacuum Systems. J Manuf Materials Processing, 2022;6(5), 98. https://doi.org/10.3390/jmmp6050098
103. Thompson MK, Moroni G, Vaneker T, Fadel G, Campbell RI, Gibson I, et al. Design for Additive Manufacturing: Trends, opportunities, considerations, and constraints. CIRP Ann Manuf Technol 2016;65:737–60. https://doi.org/10.1016/j.cirp.2016.05.004.
104. Shah J, Snider B, Clarke T, Kozutsky S, Lacki M, Hosseini A. Large-scale 3D printers for additive manufacturing: design considerations and challenges. Int J Adv Manuf Technol 2019;104:3679–93. https://doi.org/10.1007/s00170-019-04074-6.
105. Veelaert L, Du Bois E, Moons I, De Pelsmacker P, Hubo S, Ragaert K. The Identity of Recycled Plastics: A Vocabulary of Perception. Sustainability 2020;12:1953. https://doi.org/10.3390/su12051953.
106. Sauerwein M, Karana E, Rognoli V. Revived Beauty: Research into Aesthetic Appreciation of Materials to Valorise Materials from Waste. Sustainability 2017;9:529. https://doi.org/10.3390/su9040529.
107. Bridgens B, Powell M, Farmer G, Walsh C, Reed E, Royapoor M, et al. Creative upcycling: Reconnecting people, materials and place through making. Journal of Cleaner Production 2018;189:145–54. https://doi.org/10.1016/j.jclepro.2018.03.317.
108. Lithgow D, Morrison C, Pexton G, Panarotto M, Müller JR, Almefelt L, et al. Design Automation for Customised and Large-Scale Additive Manufacturing: A Case Study on Custom Kayaks. Proceedings of the Design Society: International Conference on Engineering Design 2019;1:699–708. https://doi.org/10.1017/dsi.2019.74.